Performance Analysis of Energy Storage in Smart Microgrid Based on Historical Data of Individual Battery Temperature and Voltage Changes

Irsyad Nashirul Haq*, Deddy Kurniadi, Edi Leksono, Brian Yuliarto & F.X. Nugroho Soelami

Engineering Physics Program, Faculty of Industrial Technology, Institut Teknologi Bandung, Jalan Ganesha 10, Bandung 40132, Indonesia
*E-mail: inhprop@gmail.com

Abstract. In this work, a historical data based battery management system (BMS) was successfully developed and implemented using an embedded system for condition monitoring of a battery energy storage system in a smart microgrid. The performance was assessed for 28 days of operating time with a one-minute sampling time. The historical data showed that the maximum temperature increment and the maximum temperature difference between the batteries were 4.5 °C and 2.8 °C. One of the batteries had a high voltage rate of change, i.e. above 3.0 V/min, and its temperature rate of change was very sensitive, even at low voltage rate of changes. This phenomenon tends to indicate problems that may deplete the battery energy storage system's total capacity. The primary findings of this study are that the voltage and temperature rates of change of individual batteries in real operating conditions can be used to diagnose and foresee imminent failure, and in the event of a failure occurring the root cause of the problem can be found by using the historical data based BMS. To ensure further safety and reliability of acceptable practical operating conditions, rate of change limits are proposed based on battery characteristics for temperatures below 0.5 °C/min and voltages below 3.0 V/min.

Keywords: *battery management system; energy storage system; performance analysis; smart microgrid; temperature changes; voltage changes.*

1 Introduction

The microgrid is a technology that integrates distributed energy resources, such as wind turbines, solar photovoltaic systems and energy storage systems, that have varying output power and operating conditions. Fluctuation and intermittence resulted from unstable energy sources and nonlinear loads have considerable impacts on the normal operation of a microgrid [1] and can cause volatility, high uncertainty and complexity in renewable energy generation [2]. A microgrid can operate in either grid-connected or autonomous mode [3]. In grid-connected mode it operates as a system connected to the electricity grid and can feed power to residential, commercial, or industrial loads [4]. In autonomous mode, also called off-grid or isolated mode, it can be used as back-

Received July 15th, 2018, 1st Revision December 27th, 2018, 2nd Revision January 14th, 2019 , Accepted for publication February 18th, 2019.
 ISSN: 2337-5779, DOI: 10.5614/j.eng.technol.sci.2019.51.2.1

up power supply or provide power to remote rural areas [5]. The reference voltage of a microgrid in autonomous mode is generally provided by the energy storage [5]. These operation modes and conditions may affect the reliability of distribution systems with microgrids and should be carefully investigated [6].

In isolated operational mode, voltage and frequency control are vital in microgrid systems [7]. Reference [8] proposes a voltage-based droop (VBD) control method for unbalance mitigation and sharing of distributed generation. A frequency-based control strategy has been proposed by [9] to ensure the microgrid frequency according to the strict limits imposed by the EN 50160 standard. Discussing AC/DC microgrid systems, [10] contains a comparison of microgrid systems with distributed generation (DG) systems using renewable energy sources (RES), energy storage systems (ESS) and loads. Monitoring stationary ESS is an important part of maintenance, testing, surveillance, and determination of the state of the ESS [11]. Online monitoring for fault diagnosis can also contribute to better maintenance and an optimal battery replacement program [12]. Monitoring is more important when the location is difficult to access and the efficiency of maintenance personnel needs to be ensured.

As an infrastructure of smart grids, microgrids should become even smarter in the future. A smart microgrid unifies the platform of communication for interconnection of power electronics interfaces, energy management systems, control systems and human machine interfaces (HMIs) [2]. An advantage of smart microgrids is their suitability for online visualization, data collection, and indication and manipulation of the system [13]. The most important advantage is the ability to continuously monitor the battery parameters, either during charging or discharging, which can be useful especially in battery protection systems [14]. The historical data of battery parameters are useful for maintenance as well as inspection to take possible action, either automatically or manually, to extend battery lifetime.

In order to improve the performance and extend the life of a battery energy storage systems (BESS), a battery management system (BMS) is required to deal with the dynamics of the battery system [15], while specific charge or discharge control strategies are also required [2]. The BMS will examine the operational parameters of the battery (e.g. voltage, current, and temperature) to estimate the battery state and control the charging and discharging processes [16] while maintaining safe and optimal operation of each battery [14]. BESS generate heat during rapid charge and discharge cycles at high current levels. Understanding thermal behavior and heat transfer within BESS is essential to maintain safe operating conditions [17].

The state of charge (SOC) of the battery is the most important parameter to monitor. The SOC value cannot be measured directly, but it can be estimated from measurement of several battery parameters, such as voltage, electrical current, and temperature. To determine the SOC of batteries, several approaches have been developed, which are commonly divided into two categories: electrochemical model-based methods and data-driven methods, which can eliminate the dependency of SOC estimation on physical battery models [18]. The Coulomb counting method is most commonly used to estimate the SOC, which relies on the integration of the battery current with respect to time to account for the charge added or withdrawn from the battery [16]. The traditional Coulomb counting method is preferred by most BMS manufacturers because of the assumption that all cells work at the same voltage and temperature [19]. A model-based estimation of battery SOC influenced by temperature for lithium batteries has been proposed in [20] and a combination of the Coulomb counting method with the open circuit voltage (OCV) method has been proposed in [21]. An innovative data-driven approach using an experimental dataset to predict the SOC by using support vector regression (SVR) to indicate good performance has been proposed in [22].

An advanced BMS system will monitor individual batteries inside a series configuration and identify the independent voltages and current contributions as well as the SOC levels of each battery [23]. An improved and fault tolerant voltage measurement for battery management systems has been introduced in [24]. A module-integrated distributed BMS in the battery cells without the need for an additional battery equalizer or a converter interface has been introduced in [25], and a high-efficiency BMS that applies active charge equalization to balance the charge of all cells in the pack has been proposed in [26].

In the present work, a historical data based BMS was developed and implemented using an embedded system in a smart microgrid system to monitor operating and performance conditions, including the levels of a battery pack or individual batteries that are connected in series or in parallel. The values of independent voltages, temperatures, current, and SOC levels identify and affect the operation and performance of the energy storage in the smart microgrid system. Such smart microgrid monitoring could incorporate innovative ways to visualize the power system's status and health and foresee imminent failure. In this report, individual battery voltage and temperature changes were investigated to find any potential problems and to find the sources of related problems caused by overdischarge or overcharge. The limits of acceptable practical operational conditions for battery temperature and voltage rates of change in an energy storage system were also analyzed.

2 Smart Microgrid System

The smart microgrid system used in this work is shown in Figure 1, which is deployed at the Department of Engineering Physics, Institut Teknologi Bandung, Bandung, Indonesia (latitude -6.890056 and longitude 107.609283). The system can be operated either in grid-connected or autonomous (islanding) mode and consists of a battery energy storage, a photovoltaic (PV) system, a hybrid energy controller (HEC), a grid connection, and electricity loads with two units of air conditioning systems, electronic devices, a television, and several students' laptops and computers in the Energy Management Laboratory.

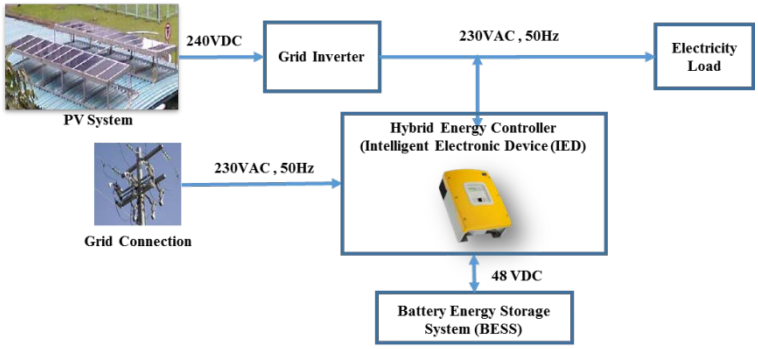

Figure 1 Smart microgrid energy layer.

The PV system's total capacity is 1000 Wp, consisting of 20 modules of ML-X 50 Wp @ 12 V, which are connected in series with an operating voltage of 240 VDC and plugged into an SMA-SB-2000 grid-tie inverter on 230 VAC/50 Hz.

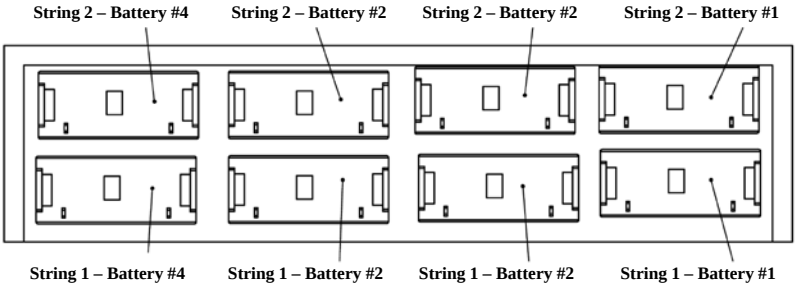

Figure 2 The battery string configuration.

The battery energy storage consists of eight valve-regulated lead acid batteries (VLRA) of LC-P12100 with characteristics as shown in Table 1, and the battery pack is configured as four batteries in series and two strings in parallel connections, as shown in Figure 2, with a nominal voltage of 48 V and a

nominal capacity of 200 Ah. Figure 3 shows the placement of the battery strings in the battery compartment. The lowest number of string connections shows the negative side of the electrical connection in the energy storage system.

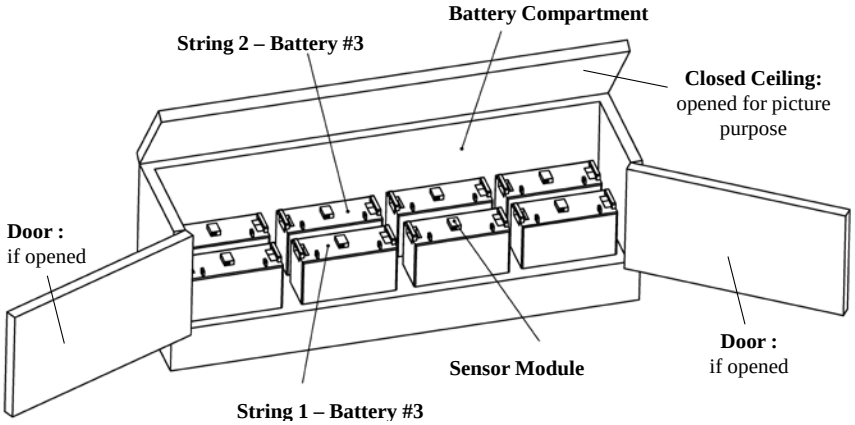

Figure 3 The battery string placement in the compartment.

The HEC used to control the energy supply and consumption in the system is operated with priority rules. These priority rules are predefined, where the energy-source management is based on the battery pack's SOC, the terminal voltage and also the energy demand [27]. The parameter configurations implemented in the HEC are shown in Tables 2 and 3. An SOC-based battery management system for microgrids has also been reported in [3]. The HEC is an SMA-SI-5048 bidirectional inverter with a nominal capacity of 5000 Wp, which is also an intelligent electronic device (IED) that provides the monitoring system to measure the battery pack system voltage, ambient temperature, and battery pack current. The HEC provides SMA-COM with proprietary serial communication to communicate to and from the devices. Using SMA-Webbox, the serial SMA-COM proprietary communication is converted to open communication protocol TCP/IP using the JavaScript object notation (JSON) format, which can be accessed to read and write parameters in the HEC.

The PV system can charge the energy storage subsequently through the PV inverter and the HEC, which may occur when there is excess power from the PV system compared to the load consumption. In order for charging to occur and run optimally, we need to convert the output of the AC voltage from the PV system or the grid to the battery's DC voltage. The DC operating and charging voltage must be adjusted to the limits and characteristics of the battery as shown in Tables 1 and 2. This arrangement can be carried out by the battery management system in the HEC.

Table 1 Battery characteristics.

Parameter	Value
Manufacturer & Model	Panasonic LC-P12100
Type & Application	VLRA, standby power
Nominal capacity (@ 25 °C)	100Ah (@ 20 hour rate)
Nominal, charge, discharge voltage	12 V; 13.6-13.8 V); 10.5 V
Operating temp. (charge; discharge)	0 to 40 °C; (-15 °C) to 50 °C
Weight	29.0 kg

Table 2 Smart microgrid operation modes by battery SOC.

Parameter	Value
SOC limit for switching (on/off) the grid	40%; 80%
Maximum battery temperature	40 °C
Voltage set point for float & full charge	13.6 & 13.8 Volt
Charging current of the battery	45 A
Set point of battery charging voltage	54.6 Volt

Table 3 Smart microgrid operation modes by load.

Parameter	Value
Activate the grid request based on power	Enable
Grid request starting; disconnecting power limit	660 W; 330 W
Nominal grid input power line current	20 Amp
Nominal power line voltage & frequency	230 VAC / 50 Hz

3 Battery Management System

In this work, a historical data based BMS was developed to provide information about the operation and performance of the individual batteries in the energy storage system. The historical data based BMS system, shown in Figure 4, is an improvement of the previous work reported in [28], consisting of a communication channel to and from the IED, sensor modules, data acquisition, local or cloud database system, and a human machine interface (HMI).

The embedded system that was developed, utilizes TCP/IP digital communication with the JSON format for data acquisition to retrieve the battery measurement parameters from the IED and utilizes USB-RS485 Modbus RTU communication to collect data from the sensor modules as the communication protocol, as implemented by [29] in a DC microgrid and by [30] for integrating data from a hybrid supply system. The Modbus communication protocol is recognized by all major device vendors as the de facto communication protocol standard [31].

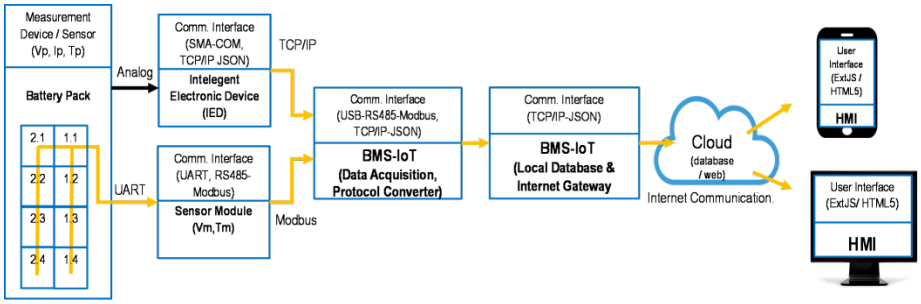

Figure 4 Smart microgrid communication layer for historical data based battery management system.

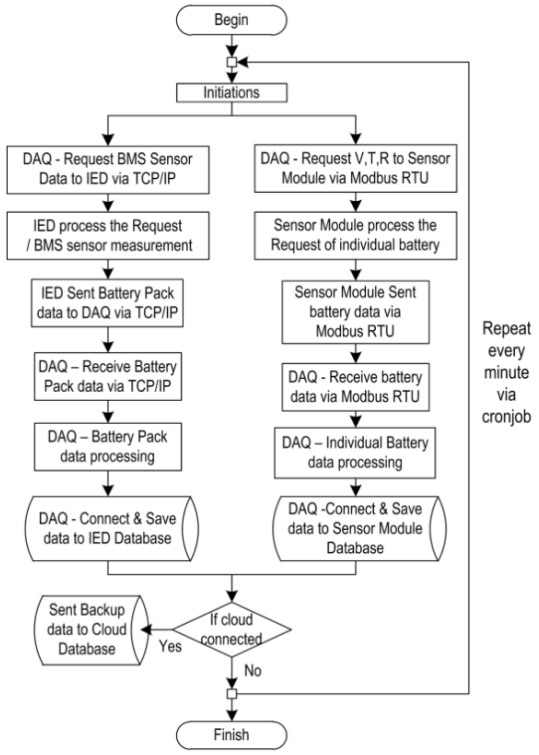

Figure 5 BMS data acquisition process.

The embedded system utilized in this work was a Raspberry Pi Model 3, a fully customizable and programmable small computer with support for a large number of peripherals and network communication [32]. Its primary function was to execute data acquisition, store and process historical data, and act as an internet gateway to the cloud server. The data acquisition algorithm in the embedded system, shown in Figure 5, is implemented using PHP and Python

server-side programming to execute two main programs. The PHP server-side program captures data from the IED TCP/IP communication, while the Python program captures data from sensor modules using the USB-RS485 Modbus RTU for every installed battery.

The sensor modules consist of voltage and temperature sensors for every battery and a UART serial communication module to Modbus RTU protocol. In this system, eight units of H3G-TA-12 calibrated voltage and temperature sensor modules were implemented and two units of TC-CTB-485 with Modbus RTU communication modules for each string connection. The individual batteries in the first string connection are represented by S1#1, S1#2, S1#3, and S1#4, while those in the second battery string connection are represented by S2#1, S2#2, S2#3, and S2#4.

To retrieve the individual battery measurement parameters from the sensor modules, the Pymodbus library in Python programming was used for reading the Modbus RTU data, which are converted to JSON format and the parameters are automatically stored in a MySQL database using structured query language (SQL). The program also executes the data acquisition to retrieve the battery pack measurement parameters from the IED in JSON format. All data are then processed and converted to SQL in corresponding columns and tables in the database system. The data acquisition is scheduled to execute every minute using Cronjob in the operating system, as mentioned in IEC Standard 61724, which is between 1 and 10 minutes per monitored data [6].

4 Results and Discussion

4.1 Battery Testing & SOC Estimation

Experimental testing was done to find the initial relationship of the battery pack voltage as a function of the SOC. New batteries were configured as in smart microgrid implementation, where four batteries were connected in series and then two strings of batteries were connected in parallel. The experiment was conducted using PowerLog 6S to monitor the voltage and current of the battery. A BK Precision 8510 (600 W) was used as programmable load controller.

The battery pack was charged until it hit the battery cut-off voltage of 54.4 V and was kept at a 60-minute rest time so that the battery pack terminal voltage approached its OCV and reached 52.07 V. This rest time is important to determine the fading of the battery capacity and also to estimate the SOC of the battery [33]. Figure 6 represents the initial or new battery pack condition for the 10 A discharging process compared to the performance of the operating

condition of the battery pack in the smart microgrid, which is correlated to its battery specifications and parameters in the HEC configuration [27].

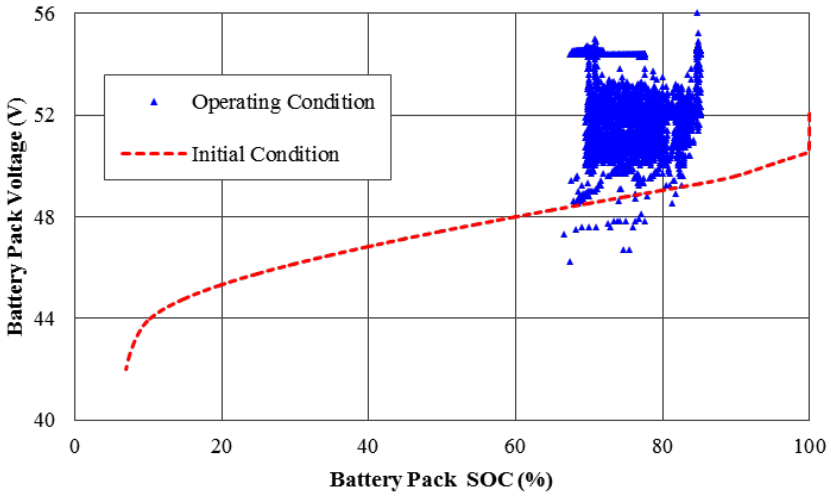

Figure 6 Relationship of battery pack terminal voltage (V) and its SOC.

Coulomb counting considering Peukert's law was used for comprehensive experimental analysis of the parameters that affect the battery discharge capacity. This formula results in a more accurate description of the discharge capacity. This phenomenon can be described using Peukert's effect, which follows Eq. (1) [34].

$$C_{disp} = T_{dis} \cdot I_{dis}^{p} \tag{1}$$

where C_{disp} is Peukert's discharge capacity in ampere-hours, T_{dis} is the discharge time, I_{dis} is the discharge current, and p is the Peukert number. When the Peukert constant is equal to 1, the discharge capacity is independent of the applied current. When k is higher than 1, the discharge capacity will decrease correlated to the discharge current.

The discrete-time SOC estimation based on Coulomb counting, which implements a compensation for Coulombic efficiency during discharging and charging, is influenced by variation of Peukert's constant. It can be expressed in Eq. (2) as in our previous research [16], stated by [35].

$$SOC_k = SOC_{k-1} + \frac{\eta_i I_{k-1} \Delta t}{C_n} \tag{2}$$

where SOC_k is the value of SOC in the k[th] discrete time interval, η_i is the Coulombic efficiency, I_{k-1} is the electricity current, which is influenced by the variation of Peukert's constant in the (k-1)[th] discrete time interval, Δt is the sampling time, and C_n is the nominal battery capacity. The Coulombic efficiency (η_i) refers to the ratio between the consumed charge when the battery is fully discharged and its corresponding available stored charge when the battery is fully charged. This ratio could be assumed to be 0.992 during the charging period and 1.0 during the discharging period [35].

The measured dynamic voltage and current with the corresponding historical data were then used to calculate the Coulomb counting to estimate the battery SOC considering the effect of Peukert's law using Eqs. (1) and (2). From the analytical calculation using Eq. (1), the initial Peukert number result was 1.2304, which correlates to Peukert's discharge current $I_k = 0.6721.I_{dis}^{1.2304}$. The initial battery pack discharge experiment was conducted from the initial battery pack voltage of 52.07 V until the voltage value hit 42.00 V, which represents the cut-off voltage for the discharge. The SOC estimation covers a range from 6% to 100% of the battery pack capacity. From the analytical results, the battery pack discharge capacity that can be drawn and used for the load was 169.98 Ah, while 30.02 Ah of battery capacity could not be used for the load because of Peukert's effect.

4.2 Energy Storage Performance Analysis

The battery pack is a power source that generates heat during rapid charge and discharge cycles at high current levels. The historical data of dynamic changes in battery voltage and temperature during charging or discharging can be used to identify potential problems and to find the sources of problems caused by overdischarge or overcharge in smart microgrid operation. In this report, the limit for acceptable practical operating conditions for the battery temperature and voltage rates of change was analyzed based on historical data using Eqs. (3) and (4).

$$\Delta T_k' = \frac{|T_k - T_{k-1}|}{\Delta t} \tag{3}$$

where $\Delta T_k'$ is the temperature rate of change at the k[th] sampling time, T_k is temperature at the k[th] sampling time, T_{k-1} is the temperature at the (k-1)[th] sampling time, and Δt is the value of the sampling time in seconds or minutes.

$$\Delta V_k' = \frac{|V_k - V_{k-1}|}{\Delta t} \tag{4}$$

where $\Delta V_k'$ is the voltage rate of changes at the k[th] sampling time, V_k is the voltage at the k[th] sampling time, V_{k-1} is the voltage at the (k-1)[th] sampling time, and Δt is the sampling time value in seconds or minutes.

4.2.1 Voltage Historical Data

Figure 7 shows the historical data of the battery pack terminal voltage and SOC (%) as a function of operating time. Several cycles of charging and discharging show anomalies. There was one operating condition in which the battery pack voltage was much lower than the others; this occurred on day 2 of the experiment. There were also two operating conditions on day 11 and 15, when the battery pack voltages were much higher than in normal conditions. Both conditions are expected to prompt problems or failure in the future because overvoltage, overcharge or overdischarge can damage a battery or shorten its useful life.

The historical data of the battery pack, as shown in Figures 6 and 7, indicate that the HEC only operates from 65% to 85% of the battery pack SOC. Under normal conditions the HEC will operate according to Tables 1 and 2, but because the battery system is already aged, where the operating conditions and battery performance have been degraded, the HEC cannot operate optimally according to predetermined parameters, which causes problems to arise during the charge or discharge process in the battery system. The SOC pack parameters were estimated by the program implemented in the HEC based on the ampere hour balance, which means that all currents flowing in and out of the battery were accumulated and referred to the nominal capacity [27] and not to the aged capacity of the battery system.

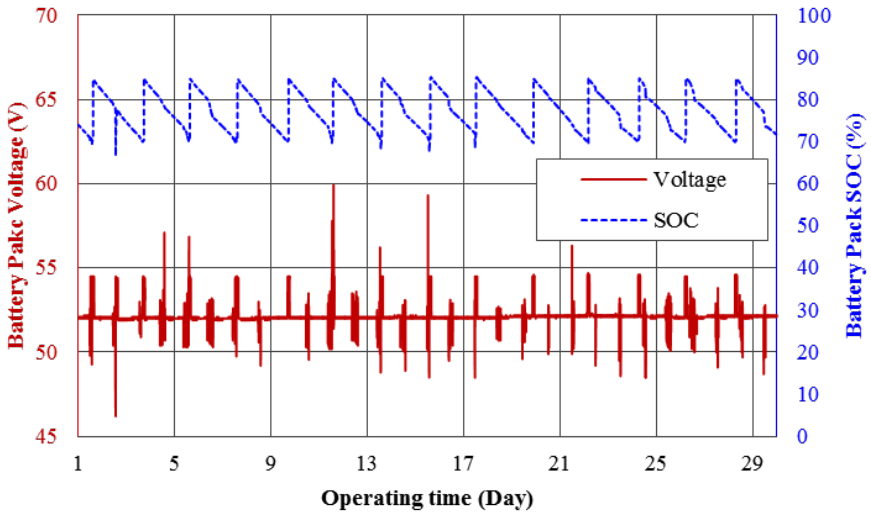

Figure 7 Historical data of battery pack terminal voltage (V) and SOC (%) as a function of operating time (day).

Because the HEC cannot monitor individual battery operation and does not have a historical information system, as one contribution in this research, a historical data based system was developed that can monitor the individual battery temperature and voltage changes. The results of the individual historical battery data are shown in Figures 8 to 11 as a function of operating time.By using the historical data of the battery cell's parameters recorded from the sensor modules in Figure 8, the source of the problem when the battery pack was under voltage or over discharge condition, as shown in Figure 7 on day 2, could be determined.

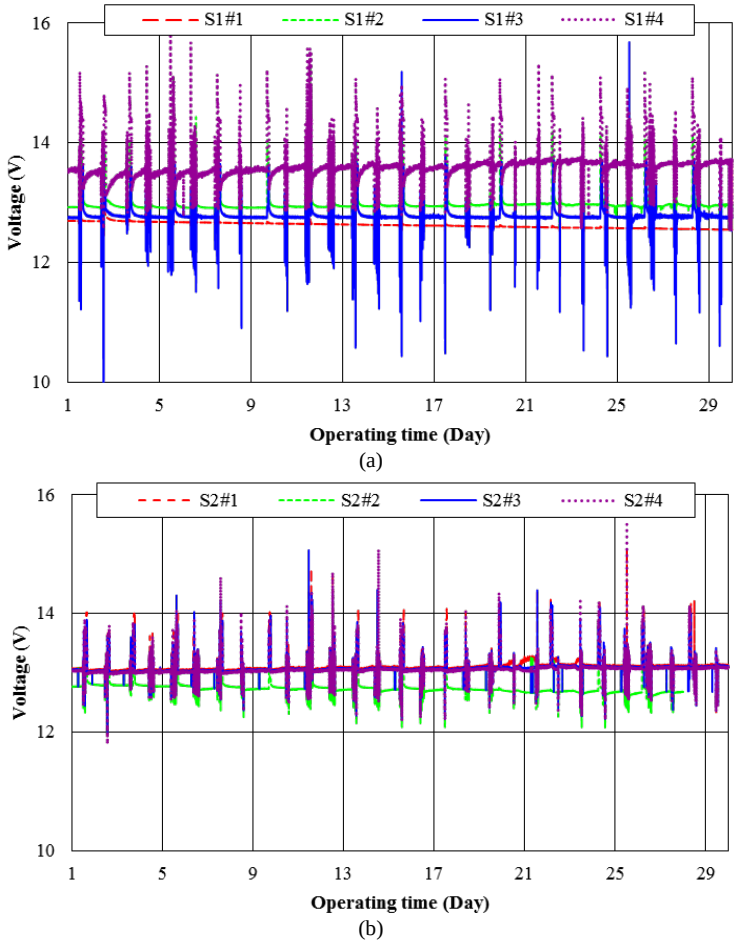

Figure 8 Historical data of batteries voltage (V) as a function of operating time, (a) string 1, (b) string 2.

Battery cells in the string 1 connection, as shown in Figure 8(a), had a much larger range of change compared to the string 2 connection in Figure 8(b). The

battery in S1#3 clearly was a strong potential source of problems, causing the energy storage to fail to operate normally, while the battery in S1#4 had a strong potential problem because of overcharging, which could cause imminent failure of smart microgrid operation.

4.2.2 Temperature Historical Data

Subsequently, based on the observation and analysis from Figure 9, the average battery temperature in the string 1 connection was slightly lower than that in string 2. This phenomenon is caused by the closed compartment/space of the battery arrangement, where the placement of the batteries in string 1 is closer to the door compared to that of string 2. In this condition, the batteries in string 1 get more ventilation compared to the batteries in string 2.

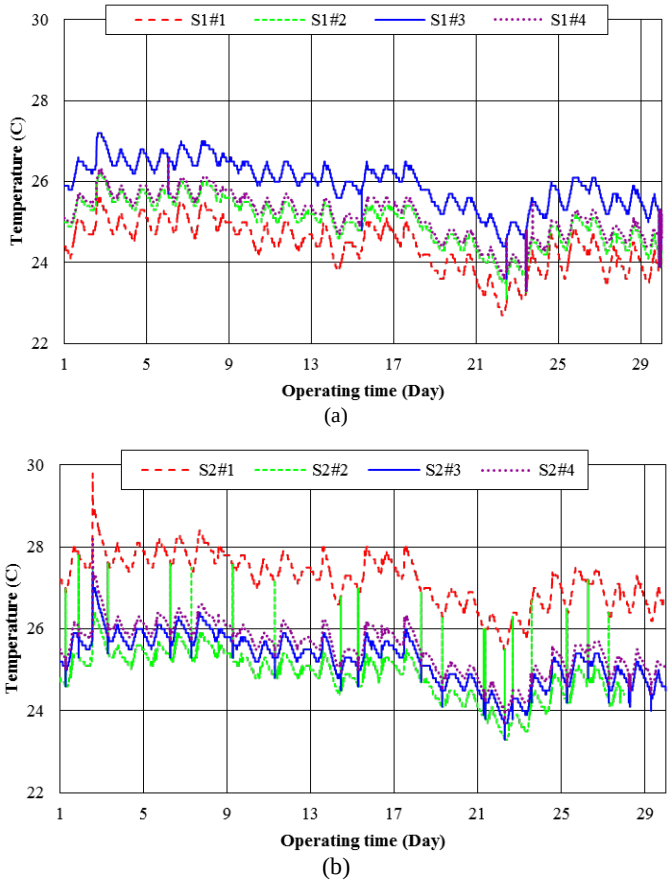

Figure 9 Historical data of battery temperature (C) as a function of operating time, (a) string 1, (b) string 2.

4.2.3 Analytical Result

The temperature relationship of each battery as a function of voltage can be seen in Figure 10. These conditions were also analyzed based on the rates of change calculated using Eqs. (3) and (4). The results can be seen in Figure 11.

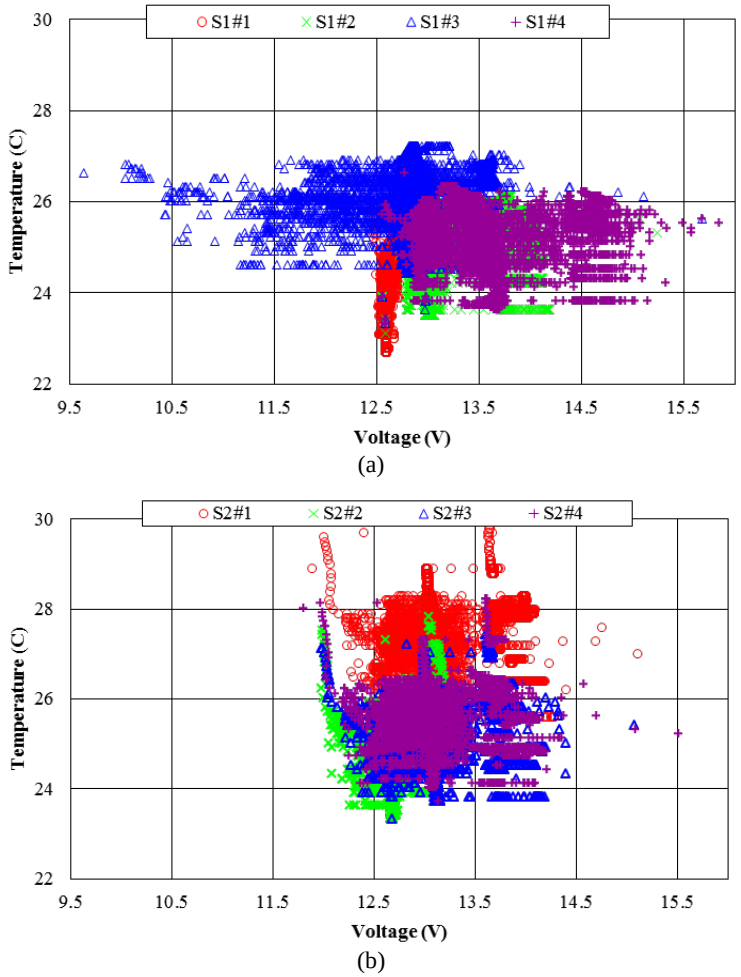

Figure 10 Relationship of individual battery temperature (C) as a function voltage, (a) string 1, (b) string 2.

The voltage of the batteries in string 1 had a significant range of changes. The temperature rate of change of battery S1#3 was even below 2.0 °C but it tended to overdischarge, which indicates a strong potential problem with the battery pack. This problem is most likely due to large voltage changes, which can be caused by the internal battery resistance being higher than that of the others

[36]. The low voltages in battery S1#3 resulted in an increase of the nearest battery voltage to compensate for the stability of the battery pack when discharge or charge processes occurred. As a result, in this case, battery S1#4 increased its voltage.

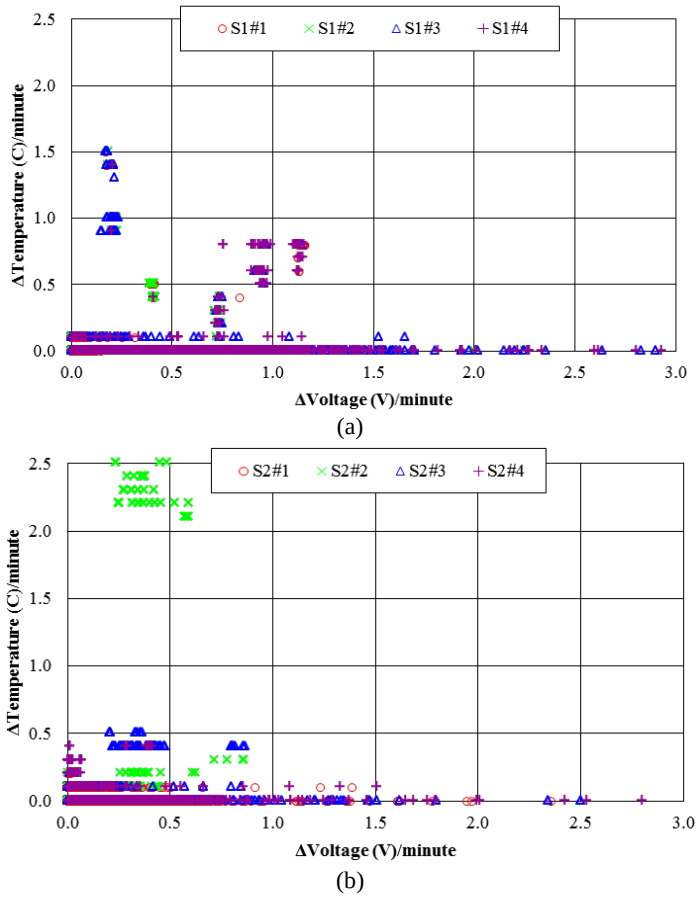

Figure 11 Battery temperature rate of change as function of voltage rate of change per minute, (a) string 1, (b) string 2.

Unlike the performance of the batteries in the string 2 connections, the relationship between voltage change and temperature change tended to be the same for the four batteries. The only difference was for S2#1, as shown in Table 5: the average battery temperature of S2#1 was 1.5 °C higher than that of the other batteries, but the dynamics tended to be similar.

There were several temperature spikes in battery S2#2, as shown in Figure 9 (b) and Figure 11 (b), where even at low voltage changes, the temperature rate of

change was above 2.0 °C. These battery temperature conditions could have been caused by failure of the battery or sensor monitoring connection [12].The analytical results indicate that the temperature changes of battery S1#3 were very sensitive to voltage changes because of the discharging process, while the temperature changes of battery S1#4 were very sensitive to voltage changes because of the charging process. From the historical data of the battery cells in the database, battery S1#3 had a voltage rate of change above 3.0 V/min, and the temperature change was very sensitive, even for a low voltage rate of change per minute. This also happened in S1#4, which had similar characteristics as S1#3. These problems tend to indicate that batteries S1#3 and S1#4 may already have reduced their battery energy storage total capacity and life cycle due to irreversible chemical reactions, as reported in [15].

In Tables 4 and 5, the maximum difference between every battery's temperature was 2.8 °C. Furthermore, the maximum temperature increment was 4.5 °C, i.e. for battery S2#4. According to [17], the maximum temperature increment and maximum temperature difference that are considered practical operating conditions for a battery pack system are below 7.61 °C and 4.29 °C.

Based on the analytical results, battery characteristics, and smart microgrid operation mode in Tables 1, 2, and 3 in this report, an acceptable temperature rate of change is below 0.5 °C/min and the voltage rate of change is below 3.0 V/min. These limitations may lead to more effective thermal management and avoid smart microgrid controller failure, which will ensure the safety and reliability of every battery used in the energy storage systems.

Table 4 Historical data of string 1 battery performance.

Battery Parameters	**V*ave* (V)**	**V*max* (V)**	**V*min* (V)**	***Tave* (°C)**	***Tmax* (°C)**	***Tmin* (°C)**
S1 #1	12.62	13.71	12.45	24.39	26.00	22.70
S1 #2	12.99	15.24	12.54	24.97	26.20	23.10
S1 #3	12.77	15.68	9.63	25.93	27.20	23.30
S1 #4	13.60	15.84	12.55	25.13	26.60	23.30
Average	13.00	15.12	11.79	25.11	26.50	23.10

Table 5 Historical data of string 2 battery performance.

Battery Parameters	**V*ave* (V)**	**V*max* (V)**	**V*min* (V)**	***Tave* (°C)**	***Tmax* (°C)**	***Tmin* (°C)**
S2 #1	13.12	15.10	11.89	27.23	29.80	25.50
S2 #2	12.73	13.26	11.97	24.88	27.80	23.30
S2 #3	13.09	15.07	11.98	25.27	27.40	23.30
S2 #4	13.07	15.51	11.80	25.55	28.20	23.70
Average	13.00	14.73	11.91	25.73	28.30	23.95

4.2.4 Smart Microgrid Power Supply Analysis

Investigations of the effects of the power supply and demand in the smart microgrid were also conducted. The battery performance diagnostic for overdischarge or the lowest voltage utilized the historical data on day 2, as shown in Figure 12. The battery pack voltage drop occurred due to the large instantaneous load change when the system was operated in isolated or islanding mode: a sudden load of over 3000 W, where the power was only supplied by the PV at less than 750 W and the rest coming from the battery pack.

In good battery energy storage performance conditions, every battery in the system should have the same voltage changes, but in this case, as shown in Figure 8 (a), battery S1#3 could not follow the same performance as the other batteries. And because the HEC is only able to operate from the battery pack's voltage and SOC to change smart microgrid operation mode, the HEC could not directly detect the condition of battery S1#3, which was already below the cut-off voltage of 10.5 V, as shown in Table 1.

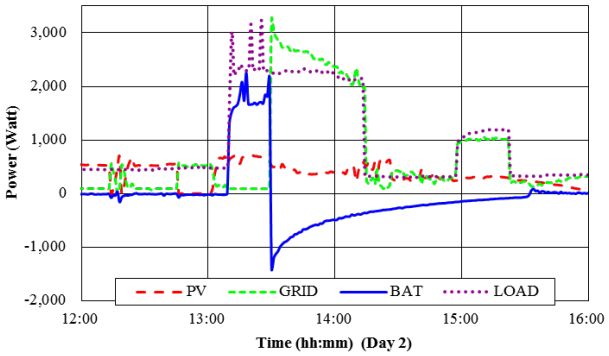

Figure 12 Power supply and demand when the lowest battery voltage occurred.

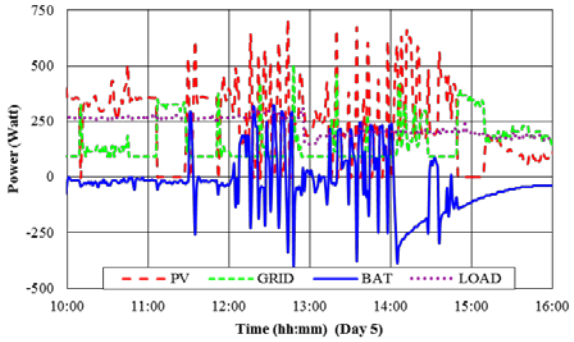

Figure 13 Power supply and demand when the highest battery voltage occurred.

The performance diagnostic for the highest individual battery voltage, which was 15.84 V on day 5, was investigated. The highly fluctuating power supply changes in the smart microgrid caused by the fluctuating power supply from the PV system are shown in Figure 13. They made the battery pack operating conditions unstable between supplying and demanding power. When the smart microgrid operated in grid connection mode, the power supply was generated by the PV system and the grid. But the weather conditions made the PV system's power generation become intermittent and unstable. This condition made the BESS operation change dynamically over a short time period between charging and discharging. The power supply fluctuation created an unbalanced voltage between the batteries in string 1 and string 2 and made battery S1#4 overcharge, creating a higher voltage compared to the other batteries.

In order to optimize and control of various energy resources, it is important to build a system that can predict the load consumption. The control system and energy storage system can be programmed with the help of reasonable prediction. Our findings are focused on real operating conditions of an energy storage system by using the voltage and temperature rates of change of individual batteries that can be diagnosed, foreseeing imminent failure and in the event of failure occurring, we can also find the root cause of the problem based on the historical BMS data. There are other findings related to this topic. For example, Ref. [37] proposed a method using energy consumption simulation and then processing the predicted data to control and optimize the energy storage system, while Ref. [38] proposed a method to manage the energy storage system by using load simulation and a variable charging/discharging threshold in order to have better load smoothing and self-consumption without the requirement of precise load or energy resource forecasting.

5 Conclusion

The smart microgrid energy storage systems operated in the SOC range from 65% to 85%, and the battery temperature changes in string number 1, row numbers 3 and 4 were very sensitive to voltage changes because of the discharging and charging processes whenever the HEC controlled the operation mode. Overdischarge or undervoltage in battery string 1 row 3 occurred because the HEC could not directly detect the battery voltage whenever it dropped below 10.5 V. Overcharge in battery string 1 row 4 occurred because of the fluctuating power generation from the PV system, which made the charging and discharging processes change dynamically over a brief period of time.

To further ensure the safety and reliability of every battery that is connected in series or in parallel in an energy storage system, limits for acceptable practical operating conditions are proposed for the battery temperature and voltage rate

of changes. An acceptable temperature rate of change based on battery characteristics and smart microgrid operation mode is below 0.5 °C/min, and the voltage rate of change is below 3 V/min. These limitations may lead to more effective thermal management and avoid smart microgrid controller failure.

Acknowledgement

The first author would like to acknowledge the Lembaga Pengelola Dana Pendidikan (LPDP), the Republic of Indonesia for providing his doctoral program scholarship. This research was partially supported by Research Grant ITB and Research Grant of Ministry of Research, Technology, and Higher Education.

References

[1] Yao, L., Yang, B., Cui, H., Zhuang, J., Ye, J. & Xue, J., *Challenges and Progresses of Energy Storage Technology and its Application in Power Systems*, J. Mod. Power Syst. Clean Energy, **4**(4), pp. 519-528, 2016.

[2] Tan, X., Li, Q. & Wang, H., *Electrical Power and Energy Systems Advances and Trends of Energy Storage Technology in Microgrid*, Int. J. Electr. Power Energy Syst., **44**(1), pp. 179-191, 2013.

[3] Miao, Z., Xu, L., Disfani, V.R. & Fan, L., *An SOC-Based Battery Management System for Microgrids*, IEEE Trans. Smart Grid, **5**(2), pp. 966-973, 2014.

[4] Malysz, P., Sirouspour, S. & Emadi, A., *An Optimal Energy Storage Control Strategy for Grid-connected Microgrids*, IEEE Trans. Smart Grid, **5**(4), pp. 1785-1796, 2014.

[5] Lu, W., Zhao, Y., Li, W. & Du, H., *Design and Application of Microgrid Operation Control System based on IEC 61850*, J. Mod. Power Syst. Clean Energy, **2**(3), pp. 256-263, 2014.

[6] Zhang, P., Li, W., Li, S., Wang, Y. & Xiao, W., *Reliability Assessment of Photovoltaic Power Systems: Review of Current Status and Future Perspectives*, Appl. Energy, **104**, pp. 822-833, Apr. 2013.

[7] Huang, X., Wang, Z. & Jiang, J., *Electrical Power and Energy Systems Control and Load-dispatching Strategies for a Microgrid with a DC / AC Inverter of Fixed Frequency*, Int. J. Electr. Power Energy Syst., **43**(1), pp. 1127-1136, 2012.

[8] Vandoorn, T.L., De Kooning, J.D.M., Van De Vyver, J. & Vandevelde, L., *Three-Phase Primary Control for Unbalance Sharing between Distributed Generation Units in a Microgrid*, Energies, **6**, pp. 6586-6607, 2013.

[9] Oureilidis, K.O., Bakirtzis, E.A. & Demoulias, C.S., *Frequency-based Control of Islanded Microgrid with Renewable Energy Sources and Energy Storage*, J. Mod. Power Syst. Clean Energy, **4**(1), pp. 54-62, 2016.

[10] Justo, J.J., Mwasilu, F., Lee, J. & Jung, J.W., *AC-microgrids versus DC-Microgrids with Distributed Energy Resources: A Review*, Renew. Sustain. Energy Rev., **24**, pp. 387-405, 2013.
[11] IEEE Power & Energy Soc., *IEEE Guide for Selection and Use of Battery Monitoring Equipment in Stationary Applications*, **1491**, IEEE, 2012.
[12] Ablay, G., *Online Condition Monitoring of Battery Systems With a Nonlinear Estimator*, IEEE Trans. Energy Convers., **29**(1), pp.232–239, Mar. 2014.
[13] Falahati, B., Fu, Y. & Mousavi, M. J., *Reliability Modeling and Evaluation of Power Systems With Smart Monitoring*, IEEE Trans. Smart Grid, **4**(2), pp. 1087-1095, 2013.
[14] Lawder, B.M.T., Suthar, B., Northrop, P.W.C., De, S., Hoff, C.M., Leitermann, O., Crow, M.L., Santhanagopalan, S. & Subramanian, V.R., *Battery Energy Storage System (BESS) and Battery Management System (BMS) for Grid-Scale Applications*, Proc. IEEE,**102**(6), 2014.
[15] Jiang, Y., Zhao, X., Valibeygi, A., de Callafon, R.A., *Dynamic Prediction of Power Storage and Delivery by Data-based Fractional Differential Models of a Lithium Iron Phosphate Battery*, Energies, **9**(8), 2016.
[16] Haq, I.N., Leksono, E., Iqbal, M., Soelami, F. X.N. & Kurniadi, D., *Development of Battery Management System for Cell Monitoring and Protection*. IEEE International Conference on Electrical Engineering and Computer Science 2014, Bali, Indonesia, pp 203–208, 2014.
[17] Xu, X.M. & He, R., *Review on the Heat Dissipation Performance of Battery Pack with Different Structures and Operation Conditions*, Renew. Sustain. Energy Rev., **29**, pp. 301–315, 2014.
[18] Wang, Y. & Orlik, P.V., *Online Battery State-of-Charge Estimation Based on Sparse Gaussian Process Regression*, IEEE Power & Energy Society General Meeting, pp. 1-4, 2016.
[19] Awadallah, M.A. & Venkatesh, B., *Accuracy Improvement of SOC Estimation in Lithium-ion Batteries*, J.Energy Storage, **6**, pp. 95-104, 2016.
[20] Xing, Y., He, W., Pecht, M. & Tsui, K.L., *State of Charge Estimation of Lithium-ion Batteries Using the Open-circuit Voltage at Various Ambient Temperatures*, Appl. Energy, **113**, pp. 106-115, 2014.
[21] Cheng, K.W.E., Divakar, B.P., Wu, H., Ding, K. & Ho, H.F., *Battery-Management System (BMS) and SOC Development for Electrical Vehicles*, IEEE Trans. Veh. Technol., **60**(1), pp. 76-88, 2011.
[22] Antón, J.C.C.A., Nieto, P.J.J.G., de Cos Juez, F.J.J., Lasheras, F.S., Vega, M.G. & Gutiérrez, M.N.N.R., *Battery State-of-charge Estimator Using the SVM Technique*, Appl. Math. Model., **37**(9), pp. 6244–6253, May 2013.
[23] Elsayed, A.T., Lashway, C.R. & Mohammed, O.A., *Advanced Battery Management and Diagnostic System for Smart Grid Infrastructure*, IEEE Trans. Smart Grid, **7**(2), pp. 897-905, 2015.

[24] Xia, B., Nguyen, T., Yang, J. & Mi, C., *The Improved Interleaved Voltage Measurement Method for Series Connected Battery Packs*, J. Power Sources, **334**, pp. 12-22, 2016.
[25] Li, Y. & Han, Y., *A Module-Integrated Distributed Battery Energy Storage and Management System*, IEEE Trans. Power Electron., **31**(12), pp. 1-1, 2016.
[26] Qian, H., Zhang, J., Lai, J.S. & Yu, W., *A High-efficiency Grid-tie Battery Energy Storage System*, IEEE Trans. Pow. Elec., **26**(3), pp. 886–896, 2011.
[27] SMA Solar Technology AG, *Off-Grid Inverter SUNNY ISLAND 5048*, TB-TEN1103, 4.0, 2015.
[28] Friansa, K., Haq, I.N., Santi, B.M., Kurniadi, D., Leksono, E. & Yuliarto, B., *Development of Battery Monitoring System in Smart Microgrid Based on Internet of Things (IoT)*, Procedia Eng., **170**, pp. 482-487, 2017.
[29] Jin, C., Wang, P., Xiao, J., Tang, Y. & Choo, F.H., *Implementation of Hierarchical Control in DC Microgrids*, IEEE Trans. Ind. Electron., **61**(8), pp. 4032-4042, 2014.
[30] Moghavvemi, M., Ismail, M. S., Murali, B., Yang, S.S., Attaran, A. & Moghavvemi, S., *Development and Optimization of a PV/diesel Hybrid Supply System for Remote Controlled Commercial Large Scale FM Transmitters*, Energy Convers. Manag., **75**, pp. 542-551, Nov. 2013.
[31] Ancillotti, E., Bruno, R. & Conti, M., *The Role of Communication Systems in Smart Grids: Architectures, Technical Solutions and Research Challenges*, Comput. Commun., **36**(17-18), pp. 1665–1697, Nov. 2013.
[32] Vujović, V. & Maksimović, M., *Raspberry Pi as a Sensor Web Node for Home Automation*, Comput. Electr. Eng., **44**, pp. 153-171, 2015.
[33] Weng, C., Cui, Y., Sun, J. & Peng, H., *On-board State of Health Monitoring of Lithium-ion Batteries Using Incremental Capacity Analysis with Support Vector Regression*, J. Power Sources, **235**, pp. 36-44, 2013.
[34] Omar, N., Bossche, P., Coosemans, T. & Mierlo, J., *Peukert Revisited – Critical Appraisal and Need for Modification for Lithium-Ion Batteries, Energies*, **6**(11), pp. 5625-5641, Oct. 2013.
[35] Mastali, M., Vazquez-Arenas, J., Fraser, R., Fowler, M., Afshar, S. & Stevens, M., *Battery State of the Charge Estimation using Kalman Filtering*, J. Power Sources, **239**, pp. 294-307, Oct. 2013.
[36] Huang, S-C., Tseng, K-H., Liang, J-W., Chang, C-L. & Pecht, M., *An Online SOC and SOH Estimation Model for Lithium-Ion Batteries*, Energies, **10**(4), p. 512, 2017.
[37] Yu, D. & Robinson, F., *Using Historical Data Processing Method to Optimize Energy Hub*, 50th Int. Univ. Power Eng. Conf., pp. 1-6, 2015.
[38] Jia, K., Chen, Y., Bi, T., Lin, Y., Thomas, D. & Sumner, M., *Historical-Data-Based Energy Management in a Microgrid with a Hybrid Energy Storage System*, IEEE Trans. Ind. Informatics, **13**(5), pp. 2597-2605, 2017.